Link Adaptation in Mobile Satellite Links: Field Trials Results

Anxo Tato, Carlos Mosquera
Signal Theory and Communications Department
University of Vigo
36310 - Vigo, Spain
Email: {anxotato,mosquera}@gts.uvigo.es

Iago Gomez
Centro Tecnoloxico de Telecomunicacions de Galicia (Gradiant)
Edificio CITEXVI, Local 14
Campus Universitario de Vigo
36310 - Vigo, Spain
Email: igomez@gradiant.org

***Abstract*—We describe the experiment that was carried out to communicate a Mobile Platform and a Ground Station through a Medium Earth Orbit (MEO) satellite. The physical layer in both ends, based on the specifications of the Satellite Component of the Universal Mobile Telecommunications System (S-UMTS), was implemented using Software Defined Radio (SDR) technology. The Mobile Terminal was boarded in both an unmanned aerial vehicle (UAV) and a car for the field trials. The ultimate goal was to test the practical performance of different physical layer adaptive techniques in the return link, and evaluate the open loop signal to noise ratio (SNR) contribution to the link adaptation algorithms.**

I. Introduction

Link adaptation is a key element of many terrestrial communication standards such as 3GPPP LTE [1], IEEE 802.16 [2] or IEEE 802.11 [3], and plays also a key role in satellite communication systems such as DVB-S2X [4], DVB-RCS2 [5] and S-UMTS [6]. The SL family of the latter standard is precisely that used as baseline for the work presented in this paper. A proprietary version of this standard is employed by the service BGAN (Broadband Global Area Network) of Inmarsat. The field trials described in this paper were developed to validate some novel link adaptation algorithms for the return link of a mobile satellite channel. Link adaptation, substantiated as Adaptive Coding and Modulation (ACM), involves the selection of the Modulation and Coding Scheme (MCS or MODCOD) of the transmitted frames according to the channel conditions with the aim of maximizing the spectral efficiency of the communications system while maintaining the error rate, measured as Frame Error Rate (FER), at a target level p_0.

Software Defined Radio (SDR) has been an essential technology for the field trials detailed in this paper. It was used to implement the physical layer of the Mobile Platform and the Ground Station, with significant effort required to achieve real time operation.

According to the SDR Forum [7], a Software Defined Radio can be defined as a radio in which some or all of the physical layer functions are software defined, so that operating functions within the radio, not just control routines, are processed by software. The radio subsystem consists only of the minimum essential RF (Radio Frequency) parts (antennas, bandpass filters, amplifiers, high frequency oscillators), an ADC (Analog to Digital Converter) and DAC (Digital to Analog Converter), together with programmable devices such as FPGAs (Field Programmable Gate Arrays) and general purpose CPUs.

The SDR platform hosting the radio subsystem was tested by setting a satellite link communicating a Mobile Terminal with a Ground Station (GS). The Mobile Terminal was flied in an UAV (Unmanned Aerial Vehicle) for some of the tests; a car was also used to test the performance for the Land Mobile Satellite (LMS) channel.

The remainder of the article is structured in the following way. In Section II a review of several adaptive schemes for link adaptation is made, with an emphasis on the algorithms implemented in the Mobile Terminal. Then, Section III deals with the practical setup of the test trials and the details of the prototype development. After that, the results are presented in Section IV and finally Section V collects the conclusions.

II. Adaptive Schemes Review

The use of ACM, by choosing different modulations and FEC (Forward Error Correction) rates, serves to avoid large link margins in time-varying channels, thus increasing the spectral efficiency for a given availability. The operation of the link adaptation schemes requires the exchange of Channel State Information (CSI) between both ends of the communication. In this paper we focus on the return link, for which the Mobile Terminal (MT) needs information about the reception at the Ground Station (GS) (see Figure 1). The algorithms that we will consider exchange the CSI and the decoding outcome in the form of acknowledgements/non-acknowledgements (ACK/NAK). As CSI, the signal to noise ratio (SNR) is the reference parameter, given its prediction capability on the result of decoding for a given MCS, provided that an accurate estimate of SNR is available. Both ends of the communication can measure the SNR; on the one hand, the closed loop CSI is the SNR measured by the Ground Station and sent back to the MT through a feedback channel. On the other hand, the open loop CSI is the SNR measured directly by the MT itself in the user downlink. If the uplink and downlink frequencies are not too far from each other in a FDD (Frequency Division Duplexing) link, then some correlation between the user uplink and the user downlink

channels is expected [8]. Therefore, the open loop CSI is an estimate of the quality of the channel that the transmissions undergo, and which is captured more precisely by the closed loop CSI. One key difference between both open loop SNR and closed loop SNR is that while the closed loop CSI arrives to the transmitter after a long delay, specially in satellite communications with GEO satellites, the open loop CSI can be used by the transmitter right after its measurement[1]. Consequently, the closed loop CSI could be completely outdated which means it does not provide useful information about the current channel conditions for rapidly variant channels, i.e., for high and moderate mobile speeds. Instead, open loop CSI, although is less precise, can still be useful in those cases.

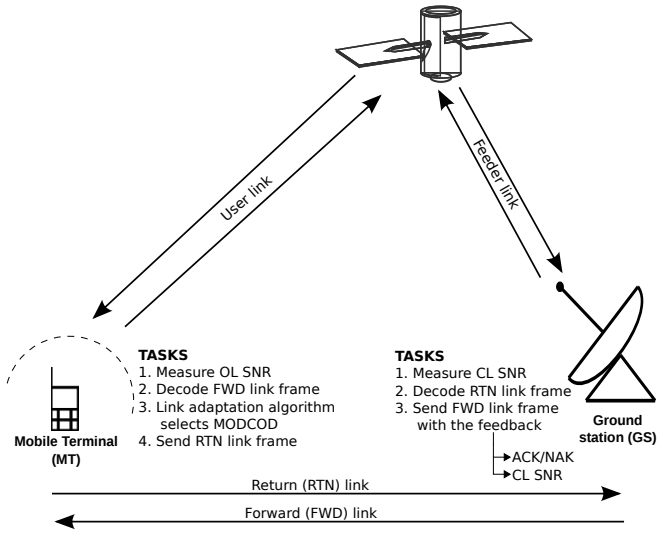

Fig. 1: Scenario of the link adaptation.

Usually, link adaptation takes place by using look-up tables (LUTs) which assign MCS to ranges of SNR values. These LUTs are built based on simulations for the fine tuning of SNR thresholds; additionally, a back-off margin is employed to account for non-ideal effects in real environments. In the algorithms that we developed and are tested in this work, this back-off margin is computed on the fly by exploiting the exchange of ACK and NAKs between the transmitter and the receiver. Furthermore, both open and closed loop CSI are combined to feed the LUT. The corresponding weight of each SNR contribution is updated with a similar algorithm to that of the margin. Overall, open loop SNR, closed loop SNR and the sequence of ACK/NAKs are used to choose the MCS at each moment, without resorting to any knowledge or assumption about the environment and channel. Note that ACM techniques can be used even in the absence of SNR information, just based on the sequence of ACK/NAKs, as reported in [9], where an algorithm named ARF-M (Automatic Rate Fallback with Memory) is introduced.

Before presenting the adaptive algorithms that we will use, we introduce a formal definition of the communication parameters. The acknowledgement of the correct decoding of the i-th codeword is denoted by ϵ_i, which takes the value 1 when the i-th codeword has not been decoded correctly (NAK) and the value 0 when it was decoded successfully (ACK). Due to the existence of a feedback delay of d frames, at time instant i the transmitter only has access to $\epsilon_0, \ldots, \epsilon_{i-d}$. The other type of feedback received by the transmitter is the closed loop SNR, $\mathrm{SNR}_i^{\mathrm{cl}}$, an estimate of the quality of the channel in time instant $i-d$ but used in time instant i due to the feedback delay. Lastly, the open loop SNR, $\mathrm{SNR}_i^{\mathrm{ol}}$, is the most recent SNR estimation on the forward link, measured in time instant $i-1$ and used in time instant i.

The transmitter selects an MCS m_i for each frame (or codeword) from a set of M available MCSs. An LUT, represented by means of a function Π, maps SNR intervals to MCS. The SNR thresholds of the LUT for each MCS are based on the required SNR needed to achieve a given FER, for example in an AWGN channel. The value of SNR introduced in the LUT for selecting the MCS is obtained by means of an equation that is different for each of the four algorithms considered here. In the sequel, all SNR parameters and margins are provided in dB. For the **closed loop algorithm** the equation is given by

$$m_i = \Pi\left(\mathrm{SNR}_i^{\mathrm{cl}} + c^{\mathrm{cl}}\right). \tag{1}$$

The corresponding **open loop** mapping is

$$m_i = \Pi\left(\mathrm{SNR}_i^{\mathrm{ol}} + c^{\mathrm{ol}}\right). \tag{2}$$

In both cases the margins should be obtained adaptively. Additionally, we consider the **balanced algorithm**, presented in [9], which selects the MCS as

$$m_i = \Pi\left(\xi^{\mathrm{ol}}\mathrm{SNR}_i^{\mathrm{ol}} + \xi^{\mathrm{cl}}\mathrm{SNR}_i^{\mathrm{cl}} + c\right), \tag{3}$$

and the **balanced convex algorithm**, with the weights adding up to one:

$$m_i = \Pi\left(\left(1-\xi^{\mathrm{cl}}\right)\mathrm{SNR}_i^{\mathrm{ol}} + \xi^{\mathrm{cl}}\mathrm{SNR}_i^{\mathrm{cl}} + c\right). \tag{4}$$

In the last two cases the weights ξ^{cl} and ξ^{ol} and the margin c are to be obtained adaptively too.

The adaptation scheme for the weights ξ and the margin c follows from an optimization problem, based on adjusting the frame error rate (FER) to an objective value p_0. The problem is solved using a stochastic gradient descent algorithm which leads to the adaptation rules (5), (6) and (7). Details of their derivation can be found in [9].

The final equation for the adaptation rule of the **balanced algorithm** reads as follows:

$$\begin{bmatrix} c_{i+1} \\ \boldsymbol{\xi}_{i+1} \end{bmatrix} = \begin{bmatrix} c_i \\ \boldsymbol{\xi}_i \end{bmatrix} - \frac{\mu}{\theta^2 + \left\|\mathbf{SNR}_{i-d}\right\|^2}\left(\epsilon_{i-d} - \tilde{p}_{0,i}\right)\begin{bmatrix} \theta \\ \mathbf{SNR}_{i-d} \end{bmatrix}, \tag{5}$$

where for simplicity we denote $\mathbf{SNR}_i = [\mathrm{SNR}_i^{cl} \;\; \mathrm{SNR}_i^{ol}]^T$ and $\boldsymbol{\xi}_i = [\xi^{cl} \;\; \xi^{ol}]^T$.

[1]Processing and buffering can delay the application of the open loop information to the transmitted frame.

In the case of the **balanced convex algorithm**, for which only one degree of freedom for the SNR weights is available, the expression for the adaptive scheme is:

$$\begin{bmatrix} c_{i+1} \\ \xi_{i+1}^{\mathrm{cl}} \end{bmatrix} = \begin{bmatrix} c_i \\ \xi_i^{\mathrm{cl}} \end{bmatrix} - \frac{\mu}{\theta^2 + \left(\mathrm{SNR}_{i-d}^{\mathrm{cl}} - \mathrm{SNR}_{i-d}^{\mathrm{ol}}\right)^2} \times \quad (6)$$
$$(\epsilon_{i-d} - \tilde{p}_{0,i}) \begin{bmatrix} \theta \\ \mathrm{SNR}_{i-d}^{\mathrm{cl}} - \mathrm{SNR}_{i-d}^{\mathrm{ol}} \end{bmatrix}.$$

As to the **open and closed loop algorithms**, the adaptation rule of the margin, the only adjustable parameter, is:

$$c_{i+1} = c_i - \frac{\mu}{\theta^2 + (\mathrm{SNR}_{i-d}^{x})^2}(\epsilon_{i-d} - \tilde{p}_{0,i}). \quad (7)$$

We need to point out that the selection of the MCS through equations (1-4) is based on the most recent values of the SNR, $\mathbf{SNR}_i$, whereas the update of $\boldsymbol{\xi}$ and c use $\mathbf{SNR}_{i-d}$, the values of SNR employed for selecting the MCS of the frame that the ACK/NAK ϵ_{i-d} refers to. This requires the transmitter to have some memory to store the values of SNR used to set the MCS of each frame until its respective ACK/NAK arrives. Furthermore, an additional loop for the variable $\tilde{p}_{0,i}$ is added, with the aim of achieving a better adjustment of the FER to p_0. The recursion for $\tilde{p}_{0,i}$ is written as

$$\tilde{p}_{0,i+1} = \tilde{p}_{0,i} - \lambda(\epsilon_{i-d} - p_0) \quad (8)$$

where $\lambda = p_0/100$. In (5), (6) and (7) $\mu = 1$ and $\theta = 10$, and in (7) x reads as $\{ol, cl\}$ for open loop and closed loop, respectively.

The margin c is restricted to lie in the interval $[-8.3, 8.3]$, whereas the weights ξ stay in the range $[0, 1]$. Thus, divergence is avoided even in the case of unattainable target FER due to, for example, poor channel conditions.

Finally, let us remark that the LUT mapping can be referred to as inner loop link adaptation, whereas the adjustment of the LUT mapping itself is known also as outer loop link adaptation in some references [10].

III. Practical Setup and Prototype

The field trials deployed a satellite communication link between a Mobile Terminal and a Ground Station. The available MCS schemes for the return link are listed in Table I, taken from [6]. On the other side, the Ground Station always employs the most robust MCS since in our trials we only want to test the algorithms for the return link. In each of the trials, the selection of the MCS for each frame was determined by one of the four link adaptation algorithms explained in the previous section. The final goal of the field trials was to compare the four algorithms in terms of spectral efficiency (throughput) and FER.

A. Satellite component

The elements of the satellite link are shown in Figure 2. The Mobile Terminal runs the link adaptation algorithms and communicates with the satellite by means of an S-band transceiver. The Ground Station, which also operates in the S-band and remains in a fixed location, sends feedback to the Mobile Terminal about the frames decoding process (ACK/NAK) and the measured SNR. The bent-pipe mode satellite is complemented by an intermediate gateway which operates in loop-back mode and is managed by the satellite operator.

For the field trials some transponder capacity from the F-2 satellite (formerly belonging to ICO) [11] was leased from the satellite operator Omnispace. The satellite operates on 30 MHz in the S band for each direction and, more specifically, it employs the range 1,985 - 2,015 MHz for the uplink and the range 2,170 - 2,200 MHz for the downlink. The communication between the satellite and the gateway is done in C-band. Although the operator owns several gateways, the teleport located in Usingen (Germany) was used for the field trials.

The end to end connection is implemented in a loop-back mode, with the gateway relaying in the uplink the signal received in the corresponding downlink after filtering and amplification. This operation mode implies that the signals travel four times the distance from the satellite to the Earth before arriving to their destination. As a result, a minimum delay of 140 ms and a round-trip-time (RTT) of 280 ms (when the elevation is 90^o) is experienced. Table II summarizes the main parameters of the involved links whereas Figure 2 numbers the sequence of hops from the Mobile Terminal to the Ground Station and the reverse.

B. Physical layer

The reference for the implementation of the physical layer was the S-UMTS standard and, in particular, the SL family [6]. This ETSI standard is conceived for providing mobile communications of third generation using GEO satellites. The frequencies employed in this standard fall in the middle of the L-band, at about 1,500-1,600 MHz. This frequency band is further divided into 200 kHz sub-bands. One important concept in its technical specification is the shared access bearers. They are physical bearers or carriers that support the transfer of data of multiple concurrent connections simultaneously, distinguishing the packets of each connection by means of their address field.

There are 13 bearers for the forward link and 22 for the return link. One bearer differs from the others in the symbol rate (and hence bandwidth), the modulation type and the slot duration. In this way, the transmission parameters can be adapted to the different channel conditions and terminal capabilities. The great flexibility provided by the large number of bearers allows data rates in the range of 3.2 to 858 kbit/s. Channels in the forward direction are allocated on a Time Division Multiplex (TDM) basis, dividing the time in slots of 80 ms. On the return direction, channels are allocated on a Time Division Multiple Access (TDMA) basis, dividing each frequency channel in small time slots being used each one by a different user. The duration of the return link time slots can be 5 ms, 20 ms or 80 ms. The system is single-carrier, and employs a root-raised-cosine (RRC) filter with roll-off

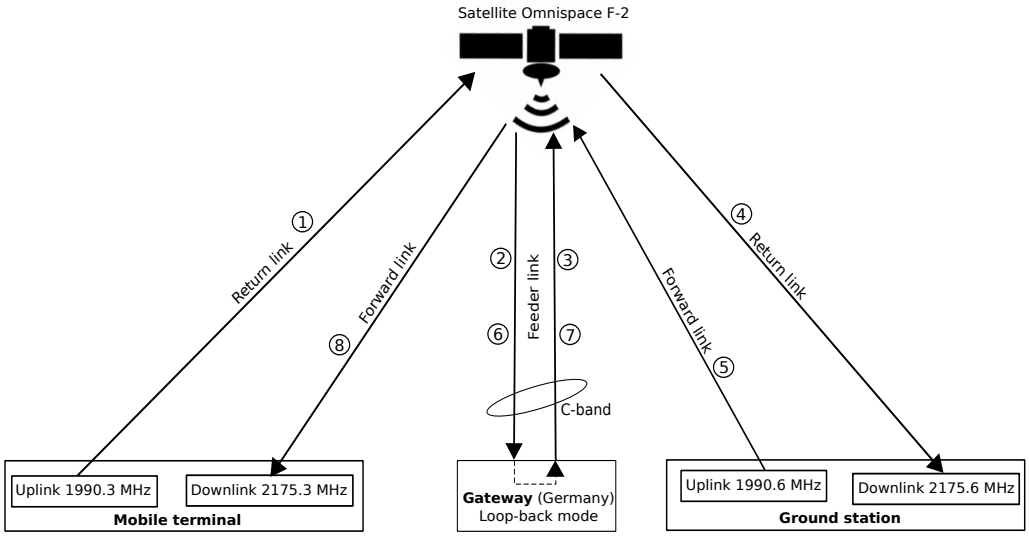

Fig. 2: Satellite links for the field trials.

TABLE I: Coding rate options for the R20T2Q-1B bearer [6], QPSK constellation.

	L8	L7	L6	L5	L4	L3	L2	L1	R	H1
Coding rate	0.33	0.41	0.48	0.55	0.63	0.71	0.78	0.84	0.87	0.91
Rate (spectral efficiency)	0.66	0.82	0.96	1.10	1.26	1.42	1.56	1.68	1.74	1.82
γ_{th} (dB)	0.03	1.03	2.03	2.93	3.73	4.83	5.83	6.73	7.43	8.33

Characteristic	**Value**
Satellite	Omnispace F-2 (former ICO F-2)
Operator	Omnispace LLC
Orbit	MEO (10,500 km) 45^o inclination
Leased bandwidth	200 kHz in each direction
Maximum EIRP (MT and GS)	43 dBm
Minimum Delay (RTT)	140 ms (280 ms)

TABLE II: Main parameters of the satellite links.

factors of 0.25 or 0.13 depending on the bearer type. Regarding channel coding, turbo-codes with variable coding rate are used in S-UMTS.

The adjustment of the communication setting takes place by first assigning a bearer type to each Mobile Terminal, and then a specific coding rate of the turbo-encoder is selected for each frame. The flexibility is somewhat limited, since several users can share a given frame, so the lowest SNR among them determines the corresponding MCS. In addition, the SNR is averaged for a long time, which entails a significant inertia for the tracking of the channel. The supported modulations range from QPSK to 64-QAM, with π/4 QPSK as an additional modulation for return link bearers. The prototype developed for this study includes bearers R20T2Q-1B (π/4-QPSK) and R20T2X-1B (16-QAM), although only the R20T2Q-1B bearer was used in the field trials for both forward and return links. The roll-off factor of the root raised cosine is 0.25 and the symbol rate is $R_s = 67.5105$ ksymb/s.

Each frame lasts 19.9 ms and contains only one FEC block which conveys 1344 slot symbols. A subgroup of symbols named Unique Word (UW), 40 at the beginning and 24 at the end of the frame, are used for frame detection, SNR estimation and frequency and phase synchronisation. They also signal the coding rate, i.e., the bearer subtype of each frame.

Figure 3 shows the block diagram of the MT transmitter. The framing block builds the base-band frames with the data and the header. This is complemented by the scrambler, the channel encoder, puncturing to generate the different coding rates, the channel interleaver, modulator and matched filter. All of these blocks are implemented following the specifications of the standard [6].

Figure 4 displays the corresponding block diagram of the MT receiver. The SDR platform has an amplifier whose gain depend on the value set by the AGC (Automatic Gain Control) block. Then, a 12 bit ADC samples the complex signal at a rate of 16 Msamples/s (giving an oversampling factor of 237). Afterwards, a decimator in the FPGA reduces the sample rate by a factor of 79 giving a sample rate at the input of the CPU of 202.532 Ksamples/s (an oversampling factor of 3). Subsequent blocks are the variable bandwidth matched filter and the DC-Offset calibration, which removes the DC component of the signal by subtracting the average of each frame. The AGC sets the power and controls the variable input amplifier. The Timing Recovery block uses the Oerder and Meyer algorithm [12] to set the optimum symbol timing. Then, the samples, now at a rate of 67.5105 Ksamples/s, can follow two different paths. During the acquisition stage, when the receiver is not locked, multiplexers (1) and (2) are in position (b). In this mode, the frame detection is

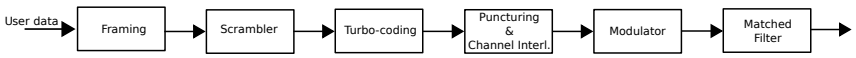

Fig. 3: Block diagram of the transmitters.

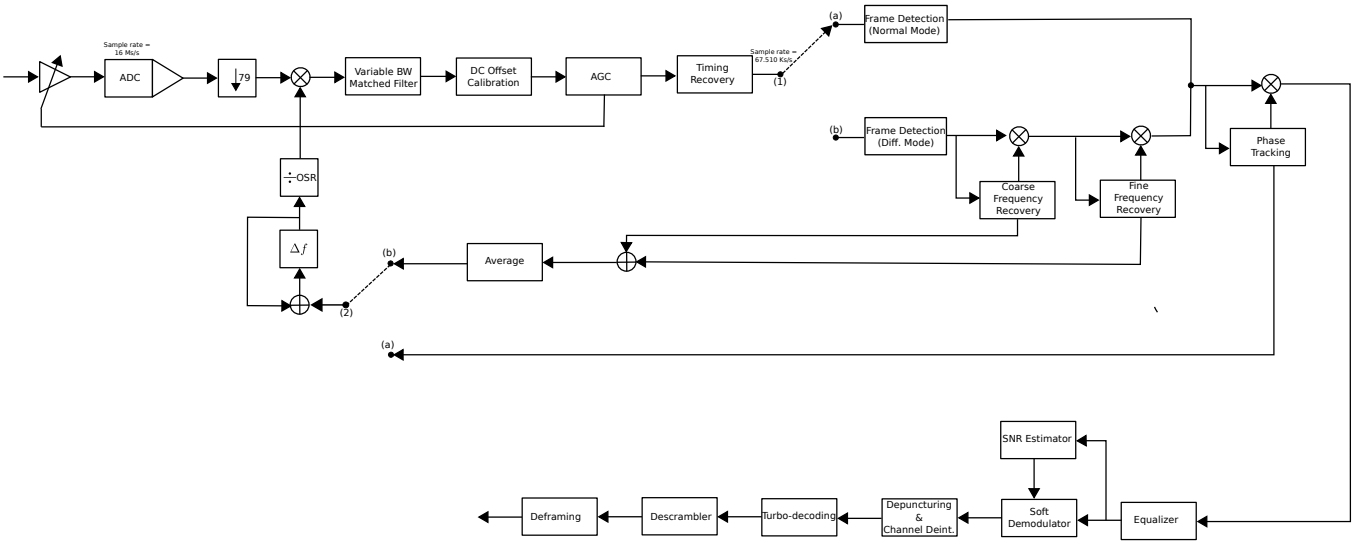

Fig. 4: Block diagram of the Mobile Terminal receiver. Tracking phase when multiplexers are in position (a) and acquisition phase when they are in position (b).

more robust, tolerating higher frequency offsets, due to the fact that the correlations are estimated based on the phase differences, as opposed to the tracking stage, with multiplexers switched to position (a). In the acquisition stage the receiver performs the frequency estimation over each frame by using the algorithm Luise&Reggiannini [13]; an average estimate is computed across several frames. In the phase tracking block, the phase is estimated at the beginning of the frame (using the first UW symbols), at the end (using the end UW symbols), and then a linear interpolation is obtained to compensate the phase error. A short adaptive FIR filter of six coefficients is also included for time equalization, by using the Multi-Modulus Algorithm [14]. The SNR Estimator block calculates the mean SNR of each frame by using a Non-Data-Aided algorithm which makes use of sixth-order statistics [15]. This estimation will be used in the soft-decoding and as a measure of the link quality. Next, the Soft Demodulator performs the soft demodulation in order to obtain the log-probabilities or LLR (Log-Likelihood Ratio). The De-puncturing, Channel De-interleaver, De-scrambler and De-framing carry out the inverse operations of their opposite blocks in the transmitter. Finally, the Turbo-decoding block decodes the signal with the BCJR algorithm. The differences between the Ground Station and the Mobile Terminal receiver lie mainly in the frame detection and the frequency recovery; for instance, in the Mobile Terminal the frame detection is easier because the Ground Station always transmits with the same MCS for this experiment.

C. Hardware

The main hardware elements of the prototypes for the MT and the GS are the SDR platform and the set of devices which form the external analog front-end. The selected SDR platform was the USRP Ettus E310 [16], which includes a dual core ARM A9 processor and a reconfigurable Xilinx 7 Series FPGA. The bulk of the baseband processing is done in a C/C++ application executed in the processor, while the FPGA implements the Intermediate Frequency up-conversion and baseband down-conversion, the decimation and the interpolation. The RF front-end of the SDR platform, the RFIC (Radio Frequency Integrated Circuit) AD 9361, includes DACs, ADCs, filters, mixers and amplifiers. Apart from the USRP, there is a transmit (TX) filter in the transmission chain, located at the transmission band to reduce the out of band emissions to avoid the contamination of the received signal. It was necessary to insert a driver, since the output power of the SDR platform is not high enough for feeding the 10 W power amplifier. Both the transmission and reception chains share the duplexer and the antenna. The duplexer connects the antenna with both transmission and reception chains. It behaves as two band pass filters, centered at the transmission and reception bands, respectively. In the reception chain there are two LNAs (Low Noise Amplifiers) and a RX filter centered in our reception frequency. This is necessary for avoiding that the power in the transmission frequency reflected in the antenna can saturate the second LNA. In order to avoid any kind of pointing and tracking in both the Mobile Terminal and the Ground Station, a hemi-directional antenna was used

in both ends. It has a beamwidth of 160^ox160^o, a gain of 2 dBiC and a right-hand circular polarization.

During the first tests it was found that the proximity of 3G base stations impaired to a large extent the decoding of the signal. This is due to the presence of strong 3G broadband signals in 2170 MHz with a power 15 dB higher than our received signal, causing the LNA of the SDR platform to saturate. The solution was to insert a fifth order helical passive band-pass filter prior to the input of the USRP able to reject the 3G interference.

D. Additional implementation details

1) Correlations: In several functional blocks of the receiver (frame detection and frequency and phase synchronization) it is necessary to compute the correlation between the received and the transmitted UW symbols. These 40 UW symbols take some predefined values according to the standard and therefore are known by the receiver. This burden can be an issue for a real time receiver since each point of the correlation requires the computation of 64 complex products (or 256 real products). By exploiting the properties of the π/4-QPSK constellation, the calculations could be simplified to a large extent, and only two real products were required for each point.

2) Variable bandwidth matched filter: Due to the large relative movement between the satellite and the Earth, systems involving MEO satellites suffer from significant Doppler. Although the Doppler of the feeder link is corrected in the gateway of Germany, our system has to cope with the Doppler shift due to the other two Earth-satellite jumps. Each jump causes approximately a shift of $\pm$10 kHz [17], giving a total shift of $\pm$20 kHz, a considerable amount if it is compared with the 84 kHz of the bandwidth of our transmitted signal. In reception, the matched filter in Figure 4 is actually a variable bandwidth low pass filter. During the acquisition phase, when the receiver is not locked, the cutoff frequency of this filter is extended so that the received signal, with a high Doppler offset, falls within the bandpass of the filter. However, during the tracking phase, when the receiver has estimated the frequency offset and has corrected it, this filter uses the nominal cutoff frequency for reducing the noise.

3) Link adaptation algorithms: The algorithms presented in Section II assume that a measurement of the open loop and a valid feedback with the closed loop SNR and the decoding outcome are always available. In practice, when the Mobile Terminal is not able to decode a frame, the values of the weights and margin remain frozen. Also, when the receivers cannot detect a frame the corresponding SNR cannot be extracted, and the value -5 dB is used instead. Additionally, when the closed loop SNR is not available, its last valid value is used in the LUT. Lastly, buffering and processing time delay the application of the open loop and the closed loop SNRs for MODCOD selection 6 frames (120 ms) and 30 frames (600 ms), respectively.

4) Link layer: In the system, due to the fact that its aim was to test the algorithms, only the essential link layer functions were implemented. Both Mobile Platform and Ground Station send a decoding flag to the other end informing about the decoding status of the frame (ACK/NAK). Future work will include improvements in this layer such as retransmissions.

5) Tracking of the Mobile Platform: The URSP Ettus E310 includes a GPS receiver and several accelerometers. The information provided by them was included as payload data for a real-time tracking of the Mobile Platform.

Fig. 5: Picture of the UAV with the Mobile Platform inside and the antenna on top.

Fig. 6: Picture of the car with the Mobile Platform on top.

IV. Results

The Mobile Platform was tested as payload of a fixed-wing UAV (see Figure 5) and on the top of a car (see Figure 6). Three different environments were tested: two terrestrial (highway and semi-rural) and one aeronautical (UAV). For each test the communication between the Mobile Platform and the Ground Station was active for five minutes. Both ends transmitted frames continuously, with the link adaptation algorithm deciding the MODCOD of each Mobile Terminal transmitted frame, whereas the Ground Station used always the most robust MODCOD for sending its feedback (ACK/NAK and closed loop SNR). The Mobile Terminal was running only one link adaptation algorithm in each trial, always with a target FER of 0.1. The transmitted power, constant during a test, was adjusted automatically at the beginning of each trial to obtain a specific average SNR at the Ground Station (a target closed loop SNR). Five different values of SNR, ranging from 0 to 12 dB, were tried.

Frame Error Rate (FER) and average spectral efficiency η of the whole transmission were calculated for each trial. The latter is defined as $\frac{1}{N}\sum_{i=1}^{N}(1-\epsilon_i)r_{m_i}$, with r_j the rate of the j-th MCS (as in Table I), and m_i the selected MCS for the transmission of i-th frame. The frames received in the Mobile Terminal with an invalid CRC (Cyclic Redundancy Check) were not taken into account for calculating neither the efficiency nor the FER, since the Mobile Terminal cannot decode correctly the information of the feedback.

The outcome of the different experiments, measured as spectral efficiency and FER, is plotted in Figure 7 as independent markers for both car and UAV. The spectral efficiency of the four adaptive schemes is similar, and all achieve the target FER for SNR values higher than 3 dB. The limitations of our platform were such that only one algorithm could be tested at a time, which made the replication of the same channel conditions a challenging task. Among other factors, the time-varying elevation of the MEO satellite introduced some complications to establish a common operation point, despite the use of the same paths for all the trials and the implementation of an initial power control. Since the time series of open and closed loop SNR values were stored, they were used off-line as input in our link adaptation simulator for a more precise and fair comparison among the four algorithms. All the algorithms were simulated first with all the available terrestrial datasets, and then the simulations were classified into five groups obtained by applying the *k-means* algorithm [18] to the average closed loop SNRs. After that, the mean efficiency and FER within each group of simulations for each algorithm were calculated. With this, the points connected with lines showed in Figure 7 are obtained. The discrepancy between the experimental and the simulated results is deemed to be caused by the abstraction of the simulation setting, working at the SNR level rather than with the waveform and assuming the perfect reception of the ACK/NAK sequence.

The first significant conclusion is that the balanced algorithm, which adapts independently closed and open loop SNR weights, offers the worst performance in terms of spectral efficiency, whereas the balanced convex version, with the two weights restricted to sum up one, outperforms slightly the other algorithms. The reason seems to be in the different number of parameters to adapt, three in the balanced scheme and two in the balanced convex one, since a higher number of adaptive parameters slow down the convergence. It can be also noticed that the performance of balanced convex, open loop and closed loop algorithms is very similar, with balanced convex marginally best and closed loop marginally worst. Although the results are not conclusive, it seems that the open loop SNR has a significant correlation with the channel state, at least comparable to that of the closed loop SNR, and possibly slightly higher. One of the potential advantages of the use of open loop SNR is the associated agility to react to quick changes in the received power; this was observed in some of the series of RSSI (Received Signal Strength Indicator) at transitions between two beams. It is also hypothesized that the open loop SNR role could be more beneficial for links with lower multipath levels, for example with directive antennas. In our experiment, the estimated values of the Rice factor (K) ranged between 14 and 16 dB.

On the other side, Figure 8 shows the temporal evolution of the closed loop SNR during an UAV flight, together with the selected MODCODs for the corresponding SNR thresholds; note how more efficient MODCODs are chosen for higher SNR values. Although the SNR range is quite low in this specific experiment, SNR values up to 12 dB were tested in other flights by adjusting the power. The right figure shows the longitude of the instantaneous position of the UAV along with the RSSI (Received Signal Strength Indicator) at the Ground Station. In this trial, where the UAV followed an elliptic trajectory, there is a strong correlation between the position of the UAV and the strength of the signal. When the UAV moves to the west, the RSSSI falls and when it moves to the east, the RSSI rises. This effect is due to the decrement in the gain of the antenna in the direction of the satellite when the UAV makes a turn to the East.

V. Conclusions

In this paper we present several link adaptation algorithms and offer details of the implementation of a satellite communication system that can be used in mobile scenarios such as vehicular and UAV communications. The field trials served to validate the correct operation of the system, and show that the open loop SNR is useful in link adaptation, since the two algorithms with marginally better performance make use of the open loop SNR. The real time implementation could not accommodate the simultaneous test of all the algorithms, and a significant effort was required to try to replicate the operation conditions for all the trials, in part due to the use of a MEO satellite, with a time-varying elevation angle. The different schemes were able to track the fluctuations of the SNR due to the variable orientation of the UAV with respect to the satellite, adapting the spectral efficiency of the communication accordingly. Lastly, this work shows also the potential of SDR technology to develop an adaptive satellite communication system and test it in real conditions.

Acknowledgement

This work was partially funded by the Spanish Government and the European Regional Development Fund under project TACTICA, by the Spanish Government under projects COMPASS (TEC2013-47020-C2-1-R), by the Galician Regional Government and the European Development Fund under projects “Consolidation of Research Units” (GRC2013/009), REdTEIC (R2014/037) and AtlantTIC. The authors would also like to thank Elena Rey and Jose Benito Dieguez for their collaboration during the development of the system and the field trials.

References

[1] “LTE; evolved universal terrestrial radio access (E-UTRA); physical layer procedures,” *ETSI TS 136 213 V8.8.0 (2009-10)*.

[2] “IEEE standard for air interface for broadband wireless access systems,” *IEEE Std 802.16-2012 (Revision of IEEE Std 802.16-2009)*, pp. 1 –2542, 17 2012.

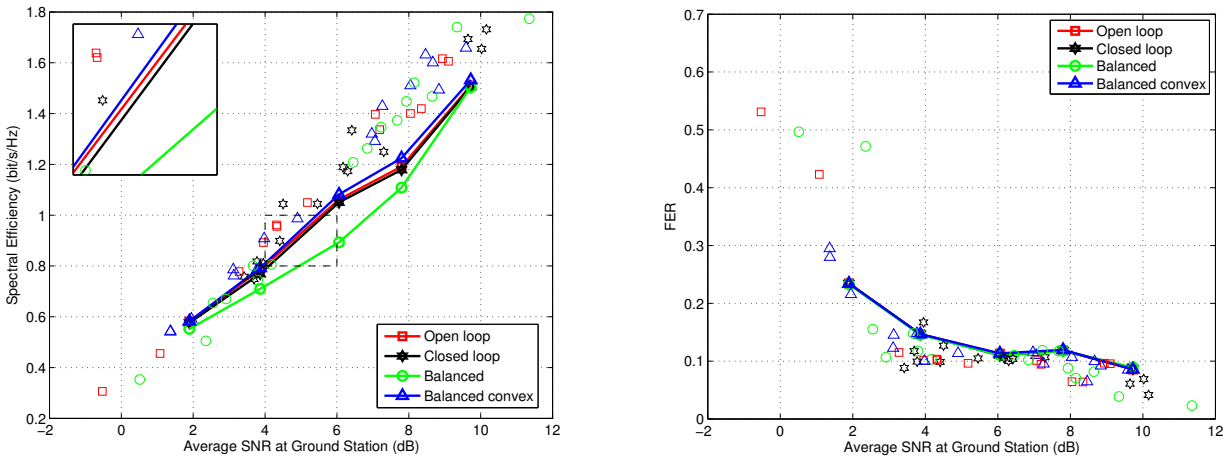

Fig. 7: Mean spectral efficiency (left) and cumulative FER (right) of field trials (independent markers) and simulations (markers connected with lines).

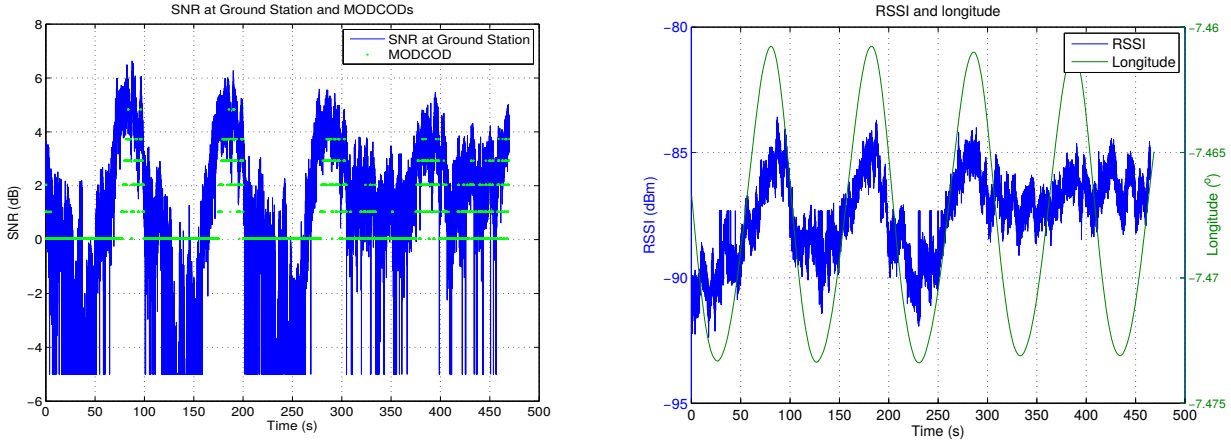

Fig. 8: Evolution of the closed loop SNR and the selected MODCODs (left), and RSSI and longitude of the UAV position (right) during one of the trials with the balanced convex algorithm.

[3] "IEEE standard for information technology–telecommunications and information exchange between systems local and metropolitan area networks–specific requirements part 11: Wireless lan medium access control (MAC) and physical layer (PHY) specifications," *IEEE Std 802.11-2012 (Revision of IEEE Std 802.11-2007)*, pp. 1–2793, 29 2012.

[4] "Digital Video Broadcasting (DVB); Second generation framing structure, channel coding and modulation systems for Broadcasting, Interactive Services, News Gathering and other broadband satellite applications; Part 2: DVB-S2 Extensions (DVB-S2X)," *ETSI EN 302 307-2 V1.1.1 (2014-10)*.

[5] "Digital video broadcasting (DVB); second generation DVB interactive satellite system (DVB-RCS2); part 1: Overview and system level specification," *ETSI TS 101 545-1 V1.1.1 (2012-05)*.

[6] "Satellite component of UMTS (S-UMTS); family SL satellite radio interface," *ETSI TS 102 744*, Oct. 2015.

[7] SDR forum. (Accessed 2016-03-30) `www.sdrforum.org`.

[8] T.-S. Yang and A. Duel-Hallen, "Adaptive modulation using outdated samples of another fading channel," in *Proc. WCNC*, vol. 1, Orlando, Florida, USA, Mar. 2002, pp. 477–481.

[9] A. Rico-Alvariño, J. Arnau, and C. Mosquera, "Link adaptation in mobile satellite links: Schemes for different degrees of CSI knowledge," *International Journal of Satellite Communications and Networking*, 2016.

[10] S. Park, R. C. Daniels, and R. W. Heath, "Optimizing the target error rate for link adaptation," in *2015 IEEE Global Communications Conference (GLOBECOM)*, Dec 2015, pp. 1–6.

[11] Omnispace. (30 of March 2016) `www.omnispacellc.com/ico-f-2/`.

[12] M. Oerder and H. Meyr, "Digital filter and square timing recovery," *IEEE Transactions on Communications*, vol. 36, no. 5, pp. 605–612, May 1988.

[13] M. Luise and R. Reggiannini, "Carrier frequency recovery in all-digital modems for burst-mode transmissions," *IEEE Transactions on Communications*, vol. 43, no. 2/3/4, pp. 1169–1178, Feb 1995.

[14] J. Yang, "Multimodulus algorithms for blind equalization," Ph.D. dissertation, University of British Columbia, Vancouver, BC, Canada, 1997.

[15] R. Lopez-Valcarce and C. Mosquera, "Sixth-order statistics-based non-data-aided snr estimation," *IEEE Communications Letters*, vol. 11, no. 4, pp. 351–353, April 2007.

[16] Ettus Research, USRP E310. (Accessed 2016-03-30) `www.ettus.com/product/details/E310-KIT`.

[17] Q. Liu, "Doppler measurement and compensation in mobile satellite communications systems," in *Military Communications Conference Proceedings, 1999. MILCOM 1999. IEEE*, vol. 1, 1999, pp. 316–320 vol.1.

[18] G. A. Seber, *Multivariate Observations*. John Wiley & Sons, Inc., 1984.